A semi-empirical formula of beach slope on flat lower platforms

Ivana M Mingo, Laurent Lacaze, Rafael Almar

Coastal Engineering 190 (2024) 104506

Contents lists available at ScienceDirect

Coastal Engineering

journal homepage: www.elsevier.com/locate/coastaleng

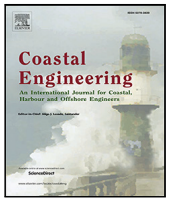

A semi-empirical formula of beach slope on flat lower platforms

Ivana M. Mingo [a,*], Laurent Lacaze [a], Rafael Almar [b]

[a] Institut de Mécanique des Fluides de Toulouse (IMFT), Université de Toulouse, CNRS, Toulouse, France
[b] LEGOS (CNRS/IRD/CNES/Toulouse University), Toulouse, France

ARTICLE INFO

Keywords:
Beach-face slope
Hydro-morphodynamics
Sediment transport
Physical modelling
Dean number
Swash zone
Low tide terrace beach

ABSTRACT

The beach slope β is a key component characterizing the coastal response to wave forcing. Here we investigate the rapid adaptation of the upper beach slope to a given wave forcing, for the case of a lower flat platform. Such types of morphology are found on coral and rocky reef beaches and low tide terrace environments. The influence of the lower platform on this rapid equilibrium beach state is shown to be significant depending on the breaking wave regime. In particular, the width of the platform and its water level can affect the wave dissipation along the inner surf and thus the wave structure entering the swash. This paper provides a classification of the beach slope equilibrium values as a function of the Dean number on a short time scale (individual wave action), based on both offshore and swash wave conditions. A decreasing trend of the beach slope with increasing offshore Dean number (Ω_0) is found for $\Omega_0 \lesssim 2.7$. For $\Omega_0 \gtrsim 2.7$ it is observed that the beach slope gradient is strongly controlled by the surf zone dissipation and it becomes necessary to define the swash Dean number (Ω_{sw}) to classify the slope. Finally, a semi-empirical formula for the beach slope evolution in the case of a low tide platform is introduced and tested on two natural low-tide terrace beaches.

1. Introduction

The swash zone is considered the most dynamic region of the coastal zone, characterized by highly unsteady and turbulent currents, large sediment transport rates and rapid morphological changes (Puleo, 2009; Kikkert et al., 2013). Understanding the dynamics of wave action therefore remains a challenge for coastal scientists, although much effort and progress has been made in recent years. Unfortunately, useful and classical models such as the Bruun rule (Bruun, 1954, 1962), the Dean equilibrium profile (Dean, 1977, 1991) or more complex cross-shore equilibrium models (Yates et al., 2009; Castelle et al., 2014; Lemos et al., 2018) are not designed to predict rapid morphological changes such as those observed in the swash zone. To improve the prediction of swash evolution, numerical models have been developed to capture the swash dynamics with different levels of complexity (Larson et al., 2004; Pritchard and Hogg, 2005; Steenhauer et al., 2012; Briganti et al., 2016, see for example). These models have been obtained and/or validated from extensive series of experimental and field measurements and are used to aid in the understanding of swash morphodynamic systems. Despite these recent advances in swash modelling, the prediction of the correct net sediment transport rates and morphological changes in the swash zone are still lacking specific details and need to be improved (Chardón-Maldonado et al., 2016; Bakhtyar et al., 2009). In addition, high quality field measurements are needed to validate and develop all these numerical models. This is a concern because field measurements of sediment transport and fluid motions in the swash zone are very difficult to obtain and analyse due to the complexity of the highly nonlinear and unsteady processes occurring simultaneously in this zone (Guza and Thornton, 1982; Puleo et al., 2003; Miles and Russell, 2004; Masselink et al., 2005; Masselink and Puleo, 2006; Turner et al., 2008). The improvements in swash knowledge will come from the development of numerical, analytical, and experimental data that will require both field and laboratory studies. This work seeks to improve the knowledge and understanding of swash dynamics by using a simplified laboratory model designed to identify, isolate, and control the specific processes that occur when approaching the swash region.

The morphology of the swash zone is characterized in part by the local beach slope (β), defined as the portion of the beach profile below the berm exposed to individual wave excursion and tidal cycles (Masselink and Li, 2001). This slope (β) is considered a key morphological parameter of swash dynamics as it affects the relative influence of wave energy dissipation and reflection at the shore, the excursion of wave run-up at the shore, and thus the direction of net sediment flux, i.e. accretion vs. erosion as sediment exchange between land and ocean (Almar et al., 2017a, 2019a,b; Martins et al., 2017). The beach slope (β) continuously adapts to changes in hydrodynamic forcing, leading to a wide range of complex feedback mechanisms between morphology and hydrodynamics (Bernabeu et al., 2003). These

* Corresponding author.
E-mail address: ivana.mingo@u-bordeaux.fr (I.M. Mingo).

https://doi.org/10.1016/j.coastaleng.2024.104506
Received 24 March 2023; Received in revised form 21 February 2024; Accepted 14 March 2024
Available online 18 March 2024

mechanisms are the drivers of hydro-sedimentary system evolution, and the complexity is given as these feedback processes are highly non-linear and scale dependent, both temporally and spatially. It is known that β responds very quickly to wave forcing from seconds, hours to days (Hughes et al., 1997; Butt and Russell, 1999; Puleo et al., 2003; Masselink and Puleo, 2006; Almeida et al., 2020), consequently the response of the beach slope to wave forcing will have an important role on the local swash dynamics and on the hydro-morphological interactions between different inner-shore zones. In order to capture the rapid fluctuations of the beach slope to changing waves, the physical model used in this study is coupled to a short time scale (several tidal cycles).

Since early research, it has been attributed by many authors that beach slope increases with increasing average sediment size (Bagnold, 1940; Masselink et al., 2016; Bascom, 1951; Turner, 1995; Reis and Gama, 2010; Bujan et al., 2019). Much effort has been invested in the relationship between beach slope and sediment size, providing a significant amount of empirical relationships for predicting the slope. Most of these expressions show a power law dependence of slope on mean sediment size, D_{50} (Sunamura, 1984; Soares, 2003; Reis and Gama, 2010). In a recent paper, Bujan et al. (2019) extracted over 2000 measurements of beach slope with associated grain sizes from available data in the literature and tested several empirical and numerical equations on this large data set. They proved that even the most representative of these equations cannot describe the full distribution of the data set. These data show a large variability of the slope (β), probably due to the wide range of data sources and therefore beach specificities, such as their instantaneous state compared to the equilibrium profile to wave forcing. The empirical relations (β-D_{50}) can therefore be used to predict the beach slope in a highly generalized form, but they still lack the physical basis to provide a clear link to swash dynamics. In particular, the strong influence of the grain diameter D_{50} on the beach slope is probably due to the sediment fall velocity, which is known to influence the transport regime relative to the wave dynamics. Following recent field results provided by Mingo et al. (2021), the present study therefore focuses on the relationship between the beach slope and the dimensionless sediment fall velocity, also known as the Dean number (β-Ω_0), based on the incoming wave characteristics.

The Dean number allows one to anticipate suspended sediment transport and direction by relating the offshore wave height (H_0) and peak period (T_0) to the sediment fall velocity (W_s). It is defined as $\Omega_0 = H_0/W_sT_0$ and can be interpreted as a dimensionless fall velocity or as a length scale ratio, since $\Omega_0 = H_0/H_g$ is the ratio of wave height to a typical height over which sediment settles during a wave period ($H_g = W_sT_o$) (Dally and Dean, 1984). Then, if $\Omega_0 = H_0/H_g \gg 1$ sediments in suspension fall to a short height compared to the spatial dimension of the wave, meaning that sediment may remain in suspension and therefore be more subject to transport between different zones of the inner beach by mean flow currents over the water depth. This is usually the case for offshore sediment transport due to return flow across the water column. On the other hand, if $\Omega_0 = H_0/H_g \ll 1$, the sediment will settle before the arrival of the next wave, so sediment transfer between zones will be limited and local morphological changes can be expected. In this case, grains remain close to the bottom, which is usually the case for onshore transport. The Dean number is more conveniently used in microtidal beaches, where the environment is wave-dominated, to classify beaches into different morphological states. Because of its link to the direction of sediment transport, global cross-shore beach profiles can be described by this dimensionless number and classified into dissipative ($\Omega_0 > 5$), intermediate ($1 < \Omega_0 < 5$), and reflective ($\Omega_0 < 1$) states. Dissipative beaches are usually characterized by a small slope β, while reflective beaches are the opposite with a steep slope (Wright et al., 1984; Short, 1996). Note that the Dean number is an important dimensionless number used in the coastal literature to classify equilibrium beach profiles on annual or seasonal time scales. The focus of this paper is to determine whether this number remains relevant for analysing swash morphology on short timescales.

Recent results obtained by analysing field data from two low tide terraces (LTT) have shown interesting correlations between the beach slope (β) and the Dean number (Mingo et al., 2021). Although these two LTT beaches have similar sediment sizes, two contrasting behaviours have been observed that stand as subclasses of the main group of low-tide terrace beaches of Wright et al. (1984). One is a swash regulated beach (SwRB) operating in a more reflective regime where the terrace is not active and energy dissipation is mainly produced in the swash zone. An active swash is observed, characterized by rapid and localized morphological changes of the beach face, the terrace becoming a consequence of the high dynamics in the swash zone. In this case, the Dean number remains lower than 2.5 ($\Omega_0 < 2.5$) and β is shown to decrease with increasing Ω_0 up to $\Omega_0 \approx 2.5$. On the other hand, the second subclass of low tide terrace beach is a surf regulated beach (SRB), where the swash zone is strongly controlled by the wave energy dissipation on the surf zone (low tide terrace). In this case, the beach was strongly affected by seasonal variations with a Dean number varying in a wide range from 1 to 6. This results in an active beach that fluctuates from a LTT dominated beach to a swash beach. When $\Omega_0 > 2.5$, the presence of LTT and its length are correlated with Ω_0, clearly highlighting SRB behaviour. When $\Omega_0 < 2.5$, the LTT disappears, suggesting a SwRB transition. Along this type of LTT beach, strongly affected by the surf, a correlation between the upper beach slope β and Ω_0, even if obtained, remains less obvious. The role of the LLT length is probably of influence here.

Following this recent relationship between the beach slope β and the Dean number Ω_0, a laboratory-scale physical model is proposed to focus on two open questions related to previous observations. (1) Is the correlation between β and Ω_0 for SwRB ($\Omega_0 < 2.5$) a universal concept associated with a direct wave-by-wave forcing on the upper part of the beach? (2) How does LTT affect the upper beach response for SRB ($\Omega_0 > 2.5$) where the swash zone may be regulated by surf zone processes?

The physical model proposed below is therefore designed to detail the response of the beach slope to single wave forcing on a short time scale. For this purpose, different initial geometric conditions are considered by varying the initial beach slope and the initial terrace length to highlight the relationship between β and Ω_0 depending on the influence of the terrace. A new beach slope predictor is then introduced for beaches with flat lower platforms. The results are discussed in relation to the aforementioned field observations of two LTT beaches, one at Nha Trang Vietnam (NT), the SRB case, and the other at Grand Popo Benin (GP), the SwRB case (Mingo et al., 2021).

2. Laboratory-scale physical model

A nearshore model is built into a laboratory wave flume. This model aims to mimic the nearshore zone at the two LTT sites Nha Trang (NT) and Grand Popo (GP), as sketched in Fig. 1. Moreover, the specific aspect of this physical model is to focus only on the swash zone and its beach slope, keeping the breaking point fixed and the surf zone non-erodible, i.e., disregarding morphological changes beyond the swash zone. This allows a simple connection between the zone of interest and its associated morphological response to the offshore wave forcing, ignoring the morphological evolution of the entire coastal zone. Since this model is mainly concerned with the evolution of the beach slope due to wave forcing, only the short time scale period is considered. According to the initial geometric position of the beach face with respect to the breaking point and the initial slope β, initial dissipative to reflective conditions can be reproduced.

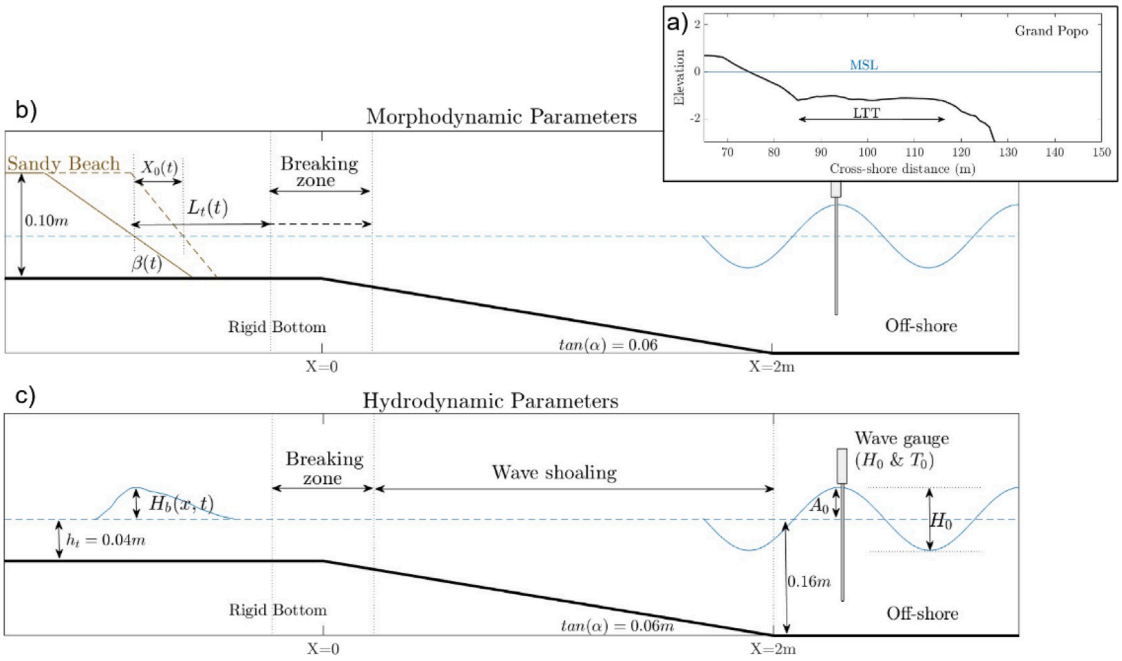

Fig. 1. Sketch of the experimental setup. (a) Mean annual cross-shore beach profile 2014 at Grand Popo. (b) Morphodynamic parameters: $\beta(t)$ is the slope of the beach face, $Lt_{sl}(t)$ is the distance from the breaking point to the shoreline, $Lt(t)$ is the distance from the breaking point to the bottom of the beach face, and $X_0((t)$ is the shoreline retreat. (c) Hydrodynamic parameters: $H_b(x,t)$ is the maximum wave amplitude after the breaking processes, H_0&T_0 wave amplitude and period at the bottom of the fixed gentle slope using a wave gauge.

2.1. Experimental set-up

The nearshore physical model is specifically designed to simulate the dynamics of the beach slope under single wave action on LTT microtidal environments. To achieve this, the model replicates the typical geometric form observed in natural beaches within these environments. As an example, Fig. 1a displays an mean annual cross-shore LTT beach profile at Grand Popo for 2014, which serves as a reference for the model's geometric design. This model is built into a unidirectional wave flume (12.65 m long, 0.3 m high, and 0.15 m wide) with an oscillating flap paddle wave generator at one end of the flume. A sketch of the experimental setup is shown in Fig. 1.

The inner shore is modelled with a rigid wave breaking mechanism to keep the breaker position fixed around $x = 0$ (x is aligned with the wave propagation along the channel). This mechanism consists of a rigid gentle slope $\tan(\alpha) = 0.06$ from $x = 2$ m to $x = 0$ then reaching a rigid horizontal platform (not erodible) for $x \leq 0$. The characteristics of the offshore wave, amplitude and period, are determined at the bottom of this fixed slope ($x = 2$) using a tide gauge (see Fig. 1); the associated wavelength is calculated using linear wave theory. The amplitude of the wave increases along the slope. For the range of offshore forcing considered along the paper, this system keeps the breaking point fixed around $x = 0$. For $x < 0$, the horizontal platform models the inner surf zone of a terraced beach. At the end of this terrace, a sloping sandy beach models the erodible beach face. The surf zone is characterized by a dissipation length, L_t, between the breaking point and the beach face. The erodible beach face, or equivalently the swash zone, consists of sand with mean size $D_{50} = 0.12$ mm and relative density $s = 2.65$. The mean sediment size (D_{50}) chosen here allows to scale the range of Dean numbers obtained in the experimental setup similarly to the field. Furthermore, the mean water depth on the terrace $H_t = 4$ cm is fixed for all experiments.

An experiment then consists of generating a monochromatic wave force, characterized by its amplitude H_0 and period T_0, for two hours starting at $t = 0$. After breaking at $x = 0$, the wave bore develop along the surf zone, of initial length $Lt(t = 0) \equiv Lt_i$ and constant depth H_t, before hitting the erodible beach surface of initial slope $\beta(t = 0) \equiv \beta_i$ (see Fig. 1). Note that the initial terrace length is also characterized by the initial distance of the shoreline position from the breaking point $Lt_{sl}(t = 0) \equiv Li_{sl}$, which is related to Li_{sl} as $Lt_{sl}(t = 0) = Lt_i + H_t/\beta_i$. Inner-surf dynamics and beach-surface morphodynamics are monitored using an optical attenuation light method, as explained later. The two hours of wave forcing correspond to about 3000 individual waves, depending on the wave period, hitting the beach face. In the field, this is in the range of a tidal cycle for wave periods around 10 s. This is therefore considered a rapid response of the beach face to a given wave forcing compared to seasonal or annual morphological changes. The specificity of the proposed model is that, depending on the initial condition of the inner-surf morphology (β_i, Lt_i) and the wave conditions (H_0, T_0), different swash and beach states, close or not to equilibrium, in either dissipative or reflective conditions, can be easily considered.

The evolution of the beach face and the dynamics of the inner surf are then characterized as a function of time and cross-shore direction by the distances of the beach face to the breaking point $Lt_{sl}(t)$ and $L_t(t)$ and the associated shoreline motion $X_0(t) = Lt_{sl}(t) - Li_{sl}$, the beach slope $\beta(t)$ and the bore height $H_b(t,x)$. High resolution sCMOS-Lavision cameras are used to extract the spatio-temporal evolving interfaces of the free surface and the sand bed. A light attenuation technique, shadowgraphy, is used for this purpose. A uniform LED backlight is placed behind the experiment, from the camera point of view, allowing to extract side views of the experiments. This allows to obtain high quality time series images of the evolution of the beach face profile and the wave evolution on the sloping fixed bottom, the terrace and the beach face. Using the optical shadowgraph technique, the evolution of the free surface $H_b(x,t)$ in the inner-surf, the beach slope $\beta(t)$ and the shoreline position $Lt_{sl}(t)$ (as defined in the sketch of Fig. 1) are extracted from the collected images. The acquisition frequency for the morphological analysis of the beach slope evolution ($\beta(t)$&$Lt_{sl}(t)$) is 2 Hz, while it is 40 Hz for the free surface extraction $h_b(x,t)$.

2.2. Wave forcing: from the wave paddle to the breaking point

When waves arrive at the nearshore, they are strongly influenced by the seabed through shoaling, resulting in a variation of the local

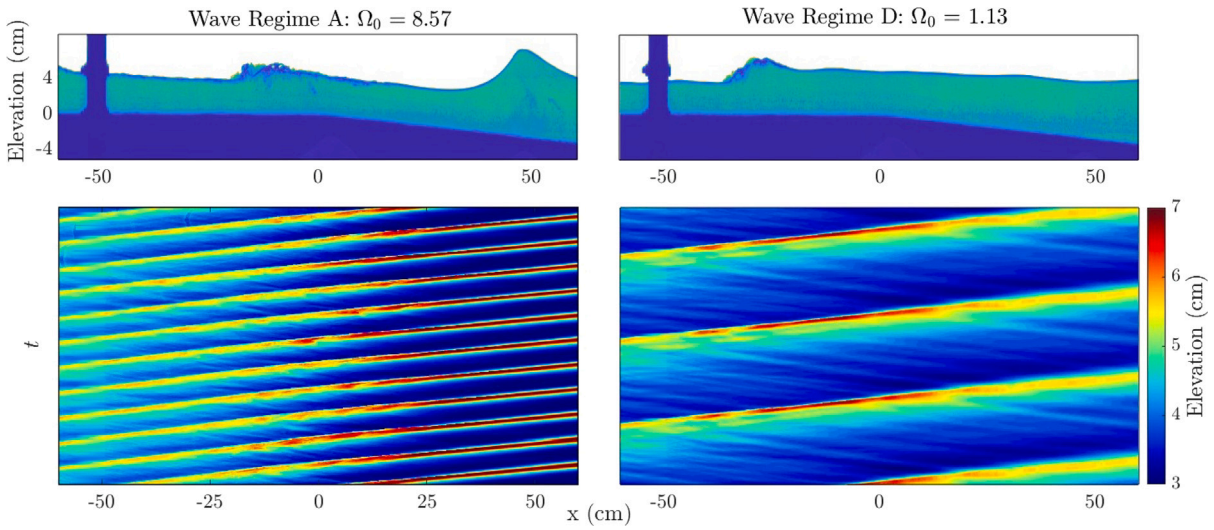

Fig. 2. The left column shows wave regime A, while the right column shows wave regime D, representing the extreme wave regimes tested. The top row shows the free surface position and elevation at a given time, highlighting two different wave breaking mechanisms. The bottom row shows the spatio-temporal diagram of the wave regime.

Table 1
Wave characteristics generated by the Wave Paddle. All parameters are extracted from wave gauge measurements at $x = 2$ m, i.e. before the rigid slope.

	H_0 [m]	T_0 [m]	λ_0 [m]	Dean number Ω_0	Wave steepness s
Wave regime A	0.047	0.74	0.75	8.58	0.062
Wave regime B	0.025	1.28	1.50	2.63	0.016
Wave regime C	0.023	1.69	2.00	2.83	0.011
Wave regime D	0.021	2.51	3.10	1.13	0.006

linear velocity leading to wave breaking, with subsequent influence on sediment transport (formation of shoals and sandbars). Changes in the bottom topography due to wave forcing produce variations in the structure of the incoming wave. These non-linear feedback interactions between waves and the seabed introduce additional space and time scale perturbations to the physical problem, affecting wave steepness, wave breaking, and consequently sediment transport at the nearshore.

In order to control this wave dynamic process in the laboratory and to maintain a constant wave forcing throughout the experiment, a non-erodible bottom with a gentle slope is introduced at a fixed distance from the wave paddle mechanism. This bottom morphology reproduces wave shoaling and keeps the breaking point fixed. The slope chosen for this rigid bottom is the result of a meticulous study carried out on the water channel, where the transformation and energy dissipation of the wave were analysed for different wave structures and rigid slopes; resulting in $tan\alpha = 0.06$ (see Fig. 1). This slope value allows to reproduce the wave shoaling in a suitable form and to reproduce different wave breaking mechanisms without losing all the wave energy during the wave shoaling, as shown in Fig. 2.

Accordingly, the wave forcing becomes one of the parameters that we can control by changing the amplitude and period of the flap paddle wave generator, leading to a well controlled propagating sinusoidal wave of amplitude H_0, period T_0 and wavelength λ_0. The four wave regimes (A–D) that have been considered along this study are given in the Table 1. As mentioned above, wave amplitude (H_0) and period (T_0) are measured with a wave gauge at the bottom of the rigid slope (see Fig. 1). The wavelength (λ_0) is calculated using the mean depth dispersion relation according to Airy wave theory. Note that the waves generated by the wave paddle are limited by the geometric size of the water channel, the type of wave generator, the rigidly sloping bottom, and the water level. The region of possible wave generation in the parameter space (H_0, λ_0) or equivalently (H_0, T_0) is shown in Fig. 3(a) together with the wave regimes considered here (symbols). As this work aims to highlight the influence of individual waves on the slope dynamics of the beach face, the wave forcing is represented by monochromatic waves. Each of the four regimes (A–D) of Table 1 and Fig. 3(a) is also characterized by its offshore wave steepness (s) and Dean number (Ω_0).

Finally, Fig. 3b shows the wave amplitude after the breaking process, i.e. at the beginning of the terrace ($H_b(x = 0)$). It is clear that the wave heights after breaking are similar for the four wave regimes tested. This means that the wave height in the inner surf zone, i.e. over the terrace, is mostly controlled by the constant water depth H_t over the terrace. This observation is consistent with the field observations reported in Almeida et al. (2020).

2.3. Inner-surf and beach slope: initial conditions and typical observations

One experiment run consists to submit an initial beach face profile, characterized by its initial slope β_i and position Lt_i, to a constant wave regime for 2 hours. The flattest initial slope β_i used is 1/20 and the steepest 1/2.5, intermediate slope of 1/7, 1/5, 1/4 where also tested. The initial position of the beach-face Li_{sl} was varied from the wave breaking point $x = 0$ up to $x = -1.3$ m by intervals of around 30 cm. A summary of the initial morphology states, wave regimes and number of experiment runs is given in Table 2. The number of runs corresponds to the number of experiments undertaken for each wave regime (A,B,C and D) varying the initial morphological conditions.

Water levels and wave forcing remain constant throughout the experiment. There is no sediment input during the experiments, i.e. the sediment available for transport corresponds only to the initial beach-face configuration. Therefore, the initial beach slope (β_i) will control whether there is more or less sediment available for transport. The beach slope can either decrease ($\beta_i > \beta_f$) or increase ($\beta_i < \beta_f$), but since there is no sediment input, the beach face position $Lt_{sl}(t)$ is mainly seen to remain unchanged or move away from the breaking point, beach erosion. Only one accretion case is observed, where the shoreline migrated towards the breaking point and was associated with a markedly flat initial beach slope ($tan\beta_i = 1/20$). This shoreline erosion or accretion is much slower than the adjustment of the beach slope and introduces a different time scale into the study.

In this experiment, we define the beach slope (β) as the linear segment of the profile encircling the mean water level on the terrace, shaped by the wave run-up and back-rush. As mentioned above, slope monitoring is accomplished by employing a high-resolution camera. The camera resolution is 18.5 px/cm, introducing a minor error of

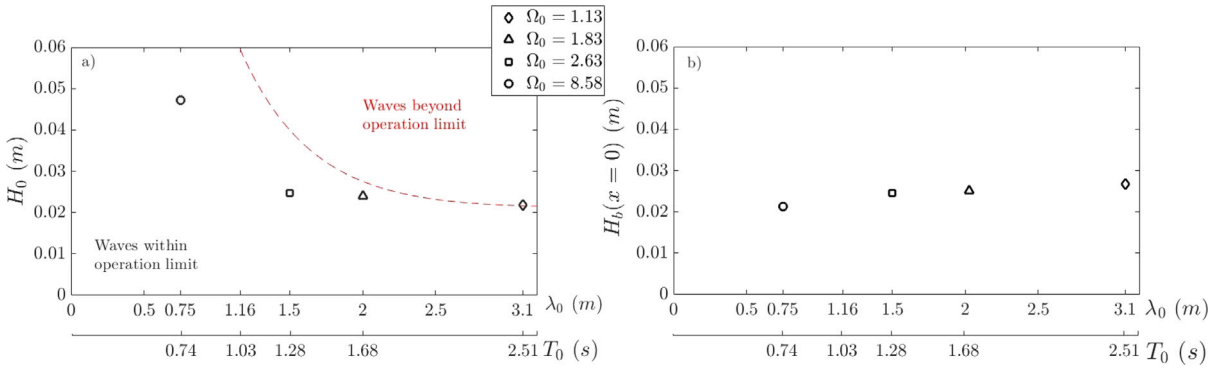

Fig. 3. (a) Operating limits of the wave generator in the parameter space of the sinusoidally propagating wave (H_0, λ_0) and (H_0, T_0). Four types of wave regimes are used in the following experiments. The wave regimes are represented by the symbols: circle, triangle, square, and diamond. Each wave regime is associated with a monochromatic wave forcing characterized by its wave amplitude (H_0), period (T_0), and wavelength (λ_0) measured with a wave gauge at the bottom of the fixed slope (see Table 1). (b) Amplitude plot Hb of the wave after breaking at $x \approx 0$ vs $T0$ and λ_0, for the same wave forcing as in figure (a).

Table 2
Set of experimental runs and initial morphological characteristics performed for each wave regime (A, B, C and D).

Wave Regime			Morphological initial conditions			Number of Runs
Type	$s = H_0/\lambda_0$	Ω_0	tan β_i	Li_{sl} (m)	Li_{sl}/H_t	
Wave Regime A	0.063	8.58	[0.06 : 0.40]	[0.10 : 1.15]	[2.50 : 28.75]	17
Wave Regime B	0.017	2.63	[0.06 : 0.40]	[0.10 : 1.30]	[2.50 : 33.75]	16
Wave Regime C	0.011	1.83	[0.05 : 0.40]	[0.10 : 1.00]	[2.50 : 25.00]	7
Wave Regime D	0.006	1.13	[0.05 : 0.40]	[0.10 : 1.30]	[2.50 : 32.50]	8

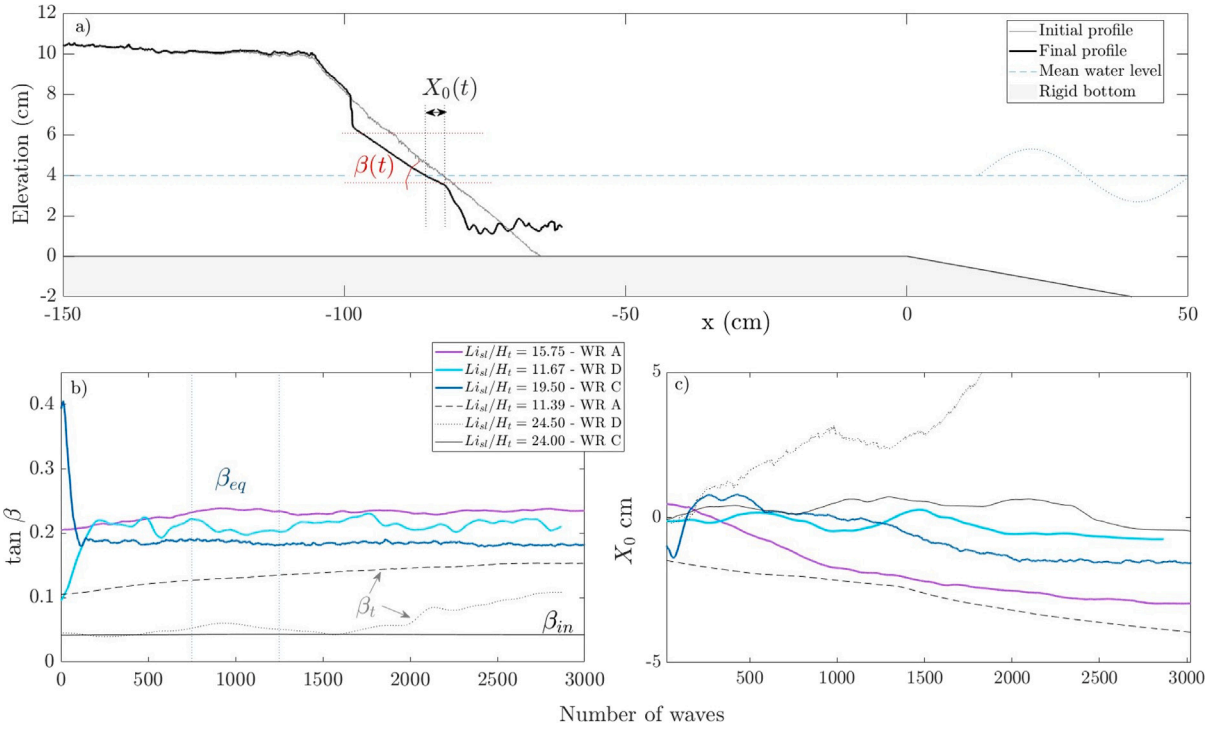

Fig. 4. (a) Initial and final position of the beach-face profile. The beach slope $\beta(t)$ defined between excursion limits of the wave (red dashed lines) surrounding the shoreline and $X_0(t)$ refers to the local shoreline position evolution. (b) 6 examples of the beach slope evolution plotted against the numbers of waves impacting the beach face: 3 cases of rapid equilibrium beach slope evolution represented by the solid blue, cyan and violet lines (β_{eq}), 2 cases of transitional beach slope states represented by dashed and dotted black lines (β_t) and 1 case of an inactive beach slope (β_{in}) represented by black line. (c) Local evolution of the beach slope position represented by the parameter X_0 associated to each beach slope rapid equilibrium experiment in Figure (b).

0.027 cm in the beach profile reconstruction. This discrepancy accounts for a 1.38% error within the wave excursion zone, which is approximately 2 cm, where the beach slope is calculated. Subsequently, we developed a post-processing code to automatically extract the beach-face slope from each image by identifying and fixing the limits of the wave excursion (refer to Fig. 4a). As the beach profile evolves over time within a single experimental run, the limits may encompass an area that could introduce a slight error in the calculation of the slope. In the worst-case scenario, this has been calculated to be 20%. However, given that each experimental test involves measuring over 2400 beach profiles, the average evolution of the slope is effectively captured and the error reduced to less than 0.9%. Therefore, the error

in the calculation of the beach slope is not taken into account in the following.

Three different situations can be identified for typical slope evolution in the present experiments. First, a fast equilibrium beach slope (β_{eq}) can be observed. In this case the slope converges to a stable value below 3000 wave impact on the beach face. This equilibrium slope corresponds to a mean value of 500 waves after convergence. Three examples of rapid equilibrium regimes for the beach slope are shown in Fig. 4b (blue, cyan, and purple solid lines). At the other end, an inactive beach slope β_{in} regime can also be observed. Here the beach face does not respond to wave forcing. An example is shown in Fig. 4b (black solid line). Finally, an intermediate state of the beach slope between the two previously described was obtained. For these cases, the slope slowly converges to its equilibrium slope, without the prior 3000 wave impact on the beach face converging. This transient state is represented by the dashed and dotted black lines in Fig. 4b.

The latter case is considered inactive in this study, as it evolves on a time scale that becomes significantly important compared to other processes observed in the field, such as seasonal variation or even intertidal water level evolution. Fig. 4c illustrates the associated local shoreline evolution, $X_0(t)$, as defined previously. Both accretive and erosive conditions are obtained on relatively long time scales compared to the rapid slope adjustment discussed here. The intermediate regime mentioned earlier is more clearly highlighted as a long time scale evolution of both slope and shoreline position, which are thus coupled. The specific analysis of this long time evolution is left to a future work, while we discuss below the rapid evolution of the slope and the associated equilibrium state. It is interesting to highlight that the equilibrium beach slope β_{eq}, as defined here, is reached in less than 1000 waves hitting the beach. This time scale could correspond to one or more tidal cycles in nature, depending on the tidal range. However, it's crucial to acknowledge that the transport regime in laboratory settings may differ from natural environments, potentially impacting the time scale of processes observed. Thus, interpreting results should consider this distinction between laboratory and field conditions.

2.4. Scaling consideration from field observations

The scaling of this experimental device is done by a geometric and physical comparison between the physical model and available field data from two low tide terrace (LTT) beaches, one at Nha Trang Vietnam and the other at Grand Popo Benin. The hydro-morphodynamics of these two LTT beaches are well described in the following papers: Lefebvre et al. (2014), Almar et al. (2014), Abessolo Ondoa et al. (2016), Almar et al. (2017b), Thuan et al. (2019), Almeida et al. (2020). The authors classified these beaches as LTT environments with similar sediment size but very different wave climate. Nha Trang (NT) is a sandy beach located in a semi-enclosed bay in southern Vietnam with a microtidal ranging from 0.4 m to 1.7 m. This beach is exposed to a low to medium energy wave climate with seasonal variability. The annual significant wave height is 0.95 m with an associated mean peak period of 6.2 s. Sediment size at NT is medium to coarse with an average grain size of 0.6 mm. Grand Popo (GP) is an open microtidal coastline forming a 500 km long mild embayment in the Gulf of Guinea. This coast is exposed to a medium to high energy wave (mean significant wave height 1.36 m; mean peak period 9.4 s), which is mostly constant over the year. Sediment size is also medium to coarse with a mean grain size of 0.6 mm.

The geometric design of the physical model used here is based on maintaining the same geometric dimensionless numbers that relate the morphology of the system to the structure of the wave. First, three dimensionless parameters are used in this scaling strategy to independently characterize the offshore wave forcing, the surf zone, and the beach face morphology. These parameters are: the ratio of offshore wave amplitude to offshore wavelength H_0/λ_0 (offshore wave forcing), the ratio of terrace length to water depth on the terrace H_t/Li_{sl} (surf zone) and the beach slope β_i (swash zone). Then, two dimensionless numbers, also based on length ratio, are defined to relate the off-shore wave structure and inner-surf morphology. They are the ratio between terrace water depth with offshore wavelength H_t/λ_0 and terrace water depth with offshore wave amplitude H_t/H_0. All these five dimensionless numbers are summarized in Table 3. As shown here, the laboratory physical model mostly preserves the geometric hydro-morphological dimensionless numbers observed at NT and GP.

A set of scaling relationships governing the physical processes of the hydro-sedimentary system is also required to increase confidence in laboratory results. However, as is often the case with complex systems, a choice has to be made on the most relevant physical process and associated dimensionless numbers to be scaled to represent field observations. In particular, a perfect similarity between laboratory and field is unattainable, since the use of the same fluid in the same gravity fields does not allow for independent variation of all physical parameters, leading to incompatibility in the scaling of all dimensionless numbers.

The physical dimensionless number used here as the most relevant to characterize beach shape is the Dean number Ω_0 discussed earlier. The range that Dean covers here is summarized in Table 4. Another relevant dimensionless number associated with sand transport under turbulent flow is the Rouse number Ro. This number (Ro) characterizes the ratio between settling velocity and the potential of the turbulent flow to set particle in suspension based on a velocity fluctuation scale associated with turbulence. In a sheared flow this velocity scale with the shear velocity induced by the mean flow. In the present case, such velocity shall scale on the bore propagation on the terrace, i.e $\propto \sqrt{gh_t}$. We thus define a characteristic Rouse number as $Ro = W_s/\sqrt{gH_t}$. In the present case an estimate of the magnitude of this number, both at the laboratory scale and in the field, is also given in Table 4. It is found to be slightly smaller than in the field. However, this value is indicative of suspended transport, which means that the transport regime remains similar in both cases. Finally, not discussed here is the Reynolds number characterizing the flow regime, which here is high enough to suggest a turbulent regime as in the field.

3. Beach slope equilibrium state

3.1. Influence of the off-shore wave forcing

We first discuss the influence of the offshore wave forcing, here characterized by the Dean number Ω_0, on the final slope β_{eq} as defined above, independent of the initial geometric conditions of the beach face (β_i&Lt_i). Both the initial slope $\tan\beta_i$ and the final slope $\tan\beta_f$ are plotted against the offshore Dean number in Fig. 5. Each symbol in Fig. 5 corresponds to an experiment. These symbols correspond to the 4 wave regimes tested (circle, square, triangle, and diamond for wave regimes A, B, C, and D, respectively). The colour map of the symbols represents their corresponding initial terrace length scaled by the terrace water depth H_t. As mentioned in Section 2.3, the intermediate state β_i is considered inactive for this analysis because it operates on a much slower time scale than the equilibrium beach slope values (β_{eq}). Then the final values of the beach slope (β_f) are either equilibrium values (β_{eq}) or inactive values (β_{in}).

In Fig. 5 two different zones of the final beach slope are identified: the equilibrium zone (β_{eq}) and the inactive zone (β_{in}). The equilibrium zone is mostly localized around $\tan\beta = 0.2$. The inactive zone is strongly associated with the morphological time scale analysed, the initial conditions of the beach face (low initial slope and beach face position far from the breaking point) and the wave forcing (wave energy injected into the system). Here it is found that it is mostly obtained for $\tan\beta < 0.1$. Then, if β_i is not in these two zones, the beach slope will rapidly evolve towards the equilibrium zone highlighted in Fig. 5(b).

Two contrasting behaviours of the beach slope are observed when classifying the equilibrium slopes (β_{eq}) using the offshore Dean number

Table 3
Geometrical dimensionless relations for the physical model and field data.

	Off-shore wave	Terrace (inner-surf)	beach slope	Hydro-morphological parameters	
	H_0/λ_0	Li_{sl}/H_t	$tan\beta_i$	H_t/λ_0	H_t/H_0
Laboratory Model					
Wave regime A	0.063	[1.06 : 33.75]	[0.05 : 0.4]	0.055	0.86
Wave regime B	0.017			0.027	1.64
Wave regime C	0.011			0.020	1.82
Wave regime D	0.0069			0.013	1.90
Nha Trang	[0.039 : 0.048]	15.5	[0.05 : 0.18]	[0.010 : 0.10]	[0.38 : 2.38]
Grand Popo	[0.011 : 0.012]	32.0	[0.10 : 0.35]	[0.0039 : 0.0140]	[0.30 : 1.44]

Table 4
Laboratory and field physical parameters.

	D_{50} [mm]	Sediment Fall velocity W_s [cm/s]	Dean $\Omega = H_0/(T_0 W_s)$	Rouse $Ro = W_s/\sqrt{gH_t}$
Laboratory model	0.12	0.74 (measured)	Wave Regime A: 8.58 Wave Regime B: 2.63 Wave Regime C: 1.83 Wave Regime D: 1.13	0.0118
NT	0.60	8.4 (Van Rijn (1993))	[1.5 : 5.0]	0.0258
GP	0.60	8.4 (Van Rijn (1993))	[1.5 : 2.5]	0.0237

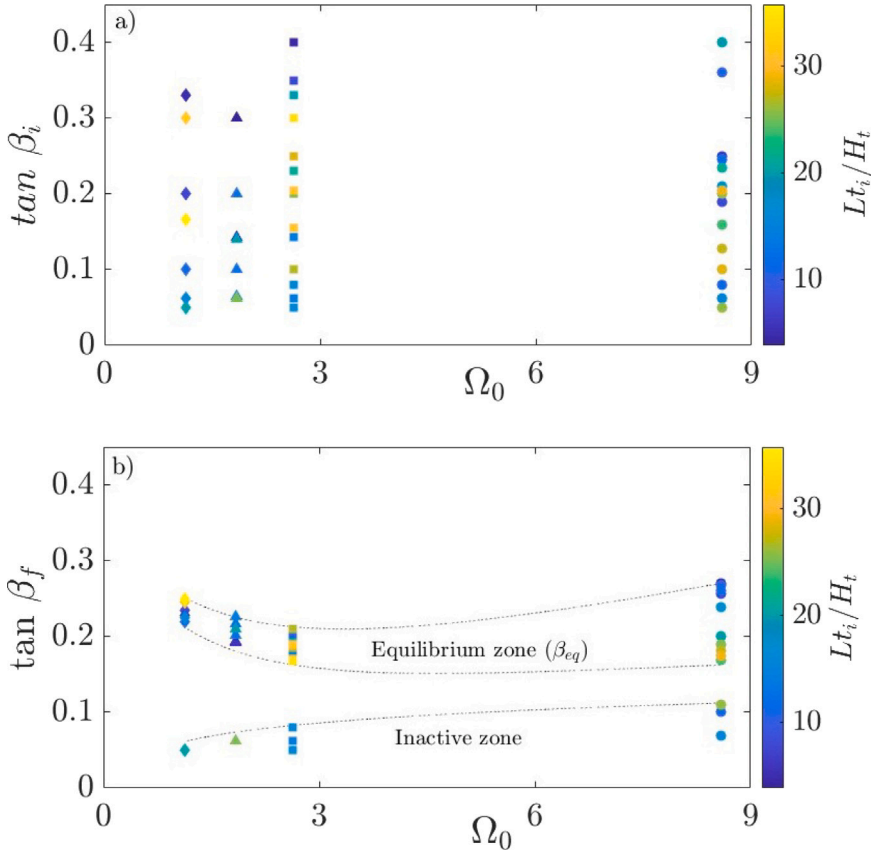

Fig. 5. Figure (a) illustrates the initial beach slope values plotted against their associated Dean number, calculated with off-shore parameters Ω_0. Figure (b) corresponds to the final values of the beach slope also plotted against their associated Dean number. Each symbol corresponds to one experiment run and the type of symbol (circle, squares, triangle and diamond) is associated to each wave regime A, B, C or D summarized in Table 2. The colour map corresponds to the initial terrace length (Lt_i/H_t).

(Ω_0), as shown in Fig. 5(b). For $\Omega_0 < 2.7$ there is an inverse relationship between β_{eq} and Ω_0, i.e. β_{eq} decreases with increasing Ω_0. In this case, a stable beach slope can be associated with the offshore wave forcing, here the Dean number Ω_0, has only a small scatter around a given $\beta_{eq}(\Omega_0)$. In particular, the terrace length does not affect the equilibrium state as defined here. These cases are observed for $\Omega_0 < 2.7$ and $\lambda_0 \gg$

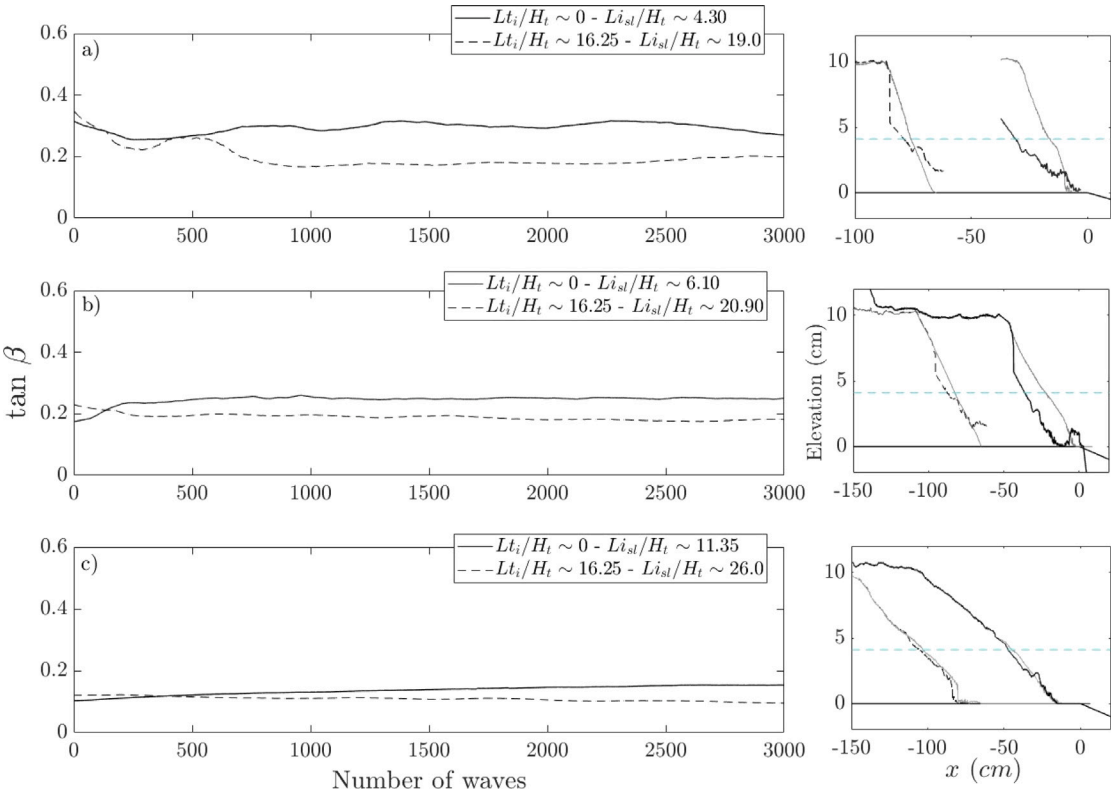

Fig. 6. Panel a, b and c show two experiments with the same initial beach slope but at two different positions from the breaking point for wave regime A. The beach slope initial positions are scaled with the water level on the terrace. The solid black lines represents the beach slope evolution for experiments starting at $Lt_i/H_t = 0$, and the dashed black line at = $Lt_i/H_t = 16.25$. Left figures show the beach slope evolution as a function of the number of waves impacting the beach-face. Right figures illustrate the initial and final beach-face profile.

L_t. On the contrary, for $\Omega_0 > 2.7$ the dispersion on β_{eq} increases with increasing Dean number. This is clearly observed for wave regime A (short wavelength and high Dean number). Nevertheless, this variation of β_{eq} at a given Ω_0, even if small, is not a random dispersion, but can be related to the terrace length. In particular, as the terrace length increases, Lt_i/H_t, β_{eq} decreases. Then, for $\Omega_0 > 2.7$, Ω_0 is not the only control parameter of the beach slope equilibrium, the surf zone dissipation now influences the final state.

To highlight the latter observation, we show the influence of the initial geometric beach face conditions (β_i&Lt_i) on the beach face dynamics for the wave regime A, i.e. $\Omega_0 = 10.7$, for which the maximum dispersion of the equilibrium beach state is obtained. The beach slope β as a function of the number of waves hitting the beach is shown in Fig. 6. In particular, each panel of Fig. 6 (a,b and c, respectively) shows the slope evolution for different initial slopes $\tan\beta_i = 0.35$, $\tan\beta_i = 0.2$ and $\tan\beta_i = 0.1$, respectively. Moreover, for each initial condition, two different initial beach face positions Lt_i, i.e. initial terrace length or equivalently surf length, are considered for each initial slope. In particular, the black lines correspond to experiments with $Lt_i = 0$, while the dashed black lines correspond to $Lt_i = 65$ cm. These lengths are given in dimensionless form in Fig. 6, using h_t as the characteristic length scale. The initial shoreline position Li_{sl}/H_t is also given for each case. Note again that Li_{sl} varies slightly with β_i as explained in Section 2.1. On the right side of each panel (a, b and c), the corresponding initial and final beach face profiles are also shown for both initial terrace lengths (grey lines correspond to the initial state and black lines correspond to the final state).

We can see that when the beach face is active (Fig. 6(a–b)), the slope $\tan\beta$ evolves to an equilibrium value that depends mostly on Li_{sl}/H_t. Then, as expected, the evolution of the beach slope depends on the terrace length. In the following, we will show that this is simply due to the wave dissipation along the inner surf zone.

3.2. Influence of the inner-surf dissipation

In order to characterize the influence of the terrace length on the wave dissipation, experiments were performed without the sandy beach. The aim of these experiments is to extract the wave transformation law after the breaking point, which is characterized by the decrease of the wave height on the flat platform (surf zone).

Fig. 7a illustrates the evolution of the maximum wave height ($H_b(x)$) on the terrace scaled by the water level on the terrace (H_t) for the 4 wave regimes. This parameter is known in the literature as the breaker index $\gamma = H_b/H_t$. At the shallow water boundary, the breaker index indicates that the breaking process begins when the wave height becomes greater than a fraction of the water depth. Accordingly, the estimation of γ at breaking can be found around $\gamma_{br} = 0.8 - -1$ in the literature (Miche, 1944; McCowan, 1891; Anon, 2021). The breaking point for the 4 wave regimes is located around $x = 0$ in the present experiments, meaning that $\gamma_{br} \equiv \gamma(x = 0)$. It is found here that γ is independent of the wave regime and has a value of $\gamma_{br} \approx 0.7$ (see Fig. 7a). Note that for wave regime A, the breaking processes occur slightly before the beginning of the terrace, i.e. for $x > 0$. However, it is observed that 4 wave regimes behave similarly for $x < 0$. In particular, the decrease of the bore height H_b/H_t along the terrace, $x < 0$, remains the same for all wave regimes. In addition, the dissipation of wave energy occurs mostly for $-15 < x/H_t < 0$. After this dissipation zone, the bore remains rather constant for the 4 wave forcings. Consequently, the height of the bores generated at the breaking point $x = 0$ and their decrease due to dissipation for $x < 0$ does not depend on the offshore wavelength and amplitude, but only on the water depth above the terrace, i.e. in the inner surf zone. From these observations, a single law of wave dissipation in the surf zone can be extracted for all wave regimes. It is found to follow an exponential decrease with distance

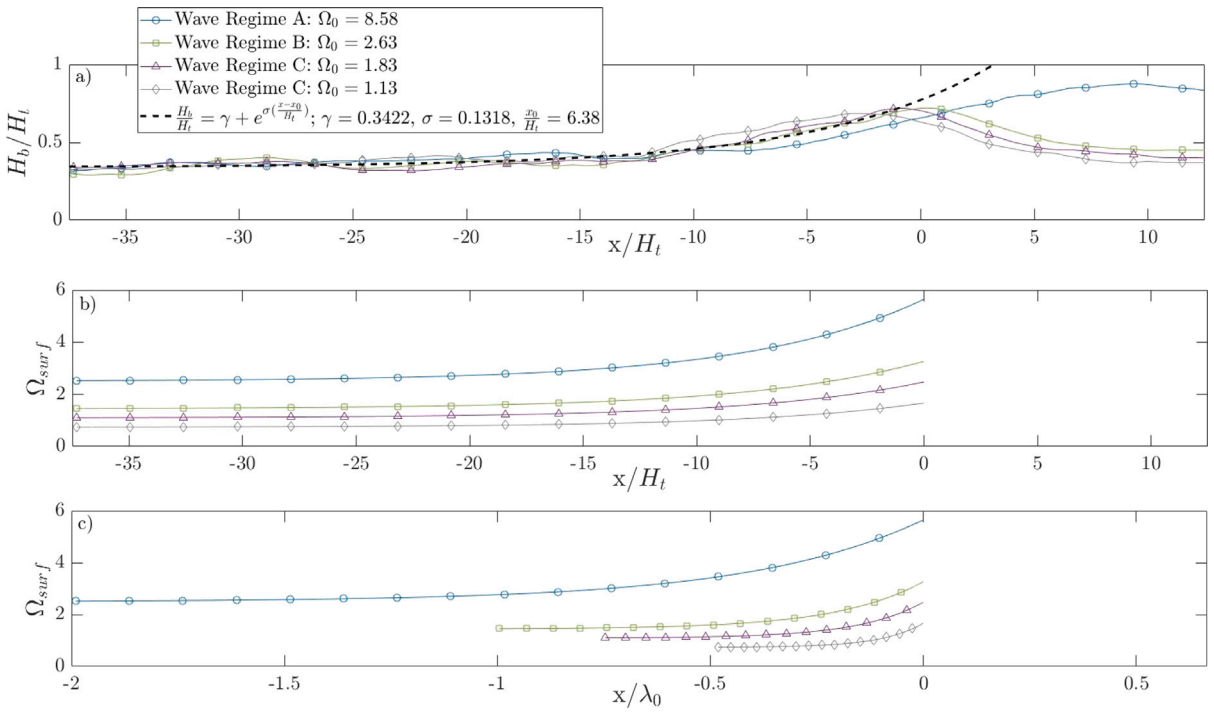

Fig. 7. (a) Wave amplitude and position on the terrace (H_b and x) are normalized by the water level on the terrace (H_t). (b) Surf Dean number evolution on the flat platform, where the position on the terrace is scaled by the water level at that point (x/H_t). (c) Surf Dean number evolution on the flat platform, where the position is scaled by the off-shore wavelength (x/λ_0).

from the breaking point, as shown by the dashed black line in Fig. 7a. It can be written as

$$\frac{H_b}{H_t} = \gamma_\infty + \exp\left[\sigma(x - x_0)/H_t\right] \quad \text{with} \quad \gamma_\infty = 0.3422; \\ \sigma = 0.1318; \quad x_0/H_t = 6.38. \tag{1}$$

Coefficients γ_0, x_0/H_t and σ are obtained using best fit of experimental data. The coefficient σ corresponds to the spatial damping rate of the bore height due to friction. The amplitude of the exponential term is assumed here to be order one as it represent the order of magnitude of the breaker criterion γ_{br}. However, an offset of the breaking point x_0/H_t is allowed as to recover the relevant γ_{br} obtained for our set of experiments. We can thus compare this solution with the breaker index (γ_{br}) at the breaking point $x = 0$. We obtain $H_b(x = 0)/Ht(x = 0) = 0.77$, which is in accordance with our previous estimation and close to values found in the literature. On the other hand, the inshore-limit of solution (1) is γ_∞, found to be 0.3422. This corresponds to the ratio of the bore height far away from the breaking point and the water height ($\gamma_\infty = H_{b\infty}/H_t$). Based on this analysis, i.e. accounting for this exponential dissipation of bore height along the inner-surf zone, a Surf Dean number can be determined, based on the local position of the bore with respect to the breaking point. It is thus defined as

$$\Omega_{surf} = \frac{H_b(x/H_t)}{T_0 W_s}. \tag{2}$$

This Surf Dean number (Ω_{surf}) accounts for the effect of wave energy dissipation through the reduction of wave amplitude on a flat platform (1). As noted in Eq. (2), the surf dean number depends on the bore height, the water level on the terrace, the offshore wave period, and the sediment fall velocity. The evolution of the Surf Dean number for the four wave regimes is shown in Fig. 7b.

3.3. Characterization of the equilibrium state based on inner-surf dissipation model

To emphasize the impact of wave dissipation due to a flat platform on the equilibrium state of the beach slope, we estimate a Swash Dean number Ω_{sw} at the bottom of the beachface Lt_i, as being the evaluation of the Surf Dean number Ω_{surf} defined in (2) at $x/H_T = -Lt_i/H_t$, i.e.

$$\Omega_{sw} = \frac{H_b(x/H_t = -Lt_i/H_t)}{T_0 W_s}, \tag{3}$$

with $H_b(x/H_t = -Lt_i/H_t)$ obtained from (1). The equilibrium slopes (β_{eq}) are thus plotted against its associated Swash Dean number Ω_{sw} in Fig. 8.

Fig. 8 shows a parabolic correlation between β_{eq} and Ω_{sw}. However, $\Omega_{sw} > 2.08$ mostly corresponds to wave regime A and $\Omega_{sw} < 2.08$ to wave regimes B, C and D. Therefore, a transition between these wave regimes is obtained at $\Omega_{sw} \approx 2.08$, which corresponds to the minimum value of β_{eq} obtained here. For $\Omega_{sw} < 2.08$, the swash mostly control the dynamics of the equilibrium beach slope. Then, even if the definition of Ω_{sw} allows a slightly better correlation with β_{eq}, it is somehow similar to Ω_0 (see Figs. 5 and 8 at small dean). However, for $\Omega_{sw} > 2.08$, the surf clearly controls the beach slope. The Swash Dean Ω_{sw} allows to explain the dispersion of β_{eq} obtained when using the Offshore Dean Ω_0. Here a unique law is obtained to classify the equilibrium beach slopes for surf and swash control cases through the transition point obtained around $\Omega_{sw} = 2.08$ or equivalently $\Omega_0 \approx 2.7$.

3.4. Application to field case

In this section, we propose a physical model to describe the evolution of the beachface slope on flat lower platforms. This model is based on either local wave action characterized by the swash Dean number (Ω_{sw}) or offshore wave action characterized by the Dean number (Ω_0). The model is tested using wave parameters extracted from field data at two LTT beaches, Nha Trang (NT) and Gran Popo (GP), which corresponds to the same field data used to scale the experimental device. The results of the model are then compared to the beachface slope evolution at NT and GP extracted from the long time series field experiments surveys.

The field data collection spanned from 2013 to 2016 and was obtained via video systems validated by short-term field experiments

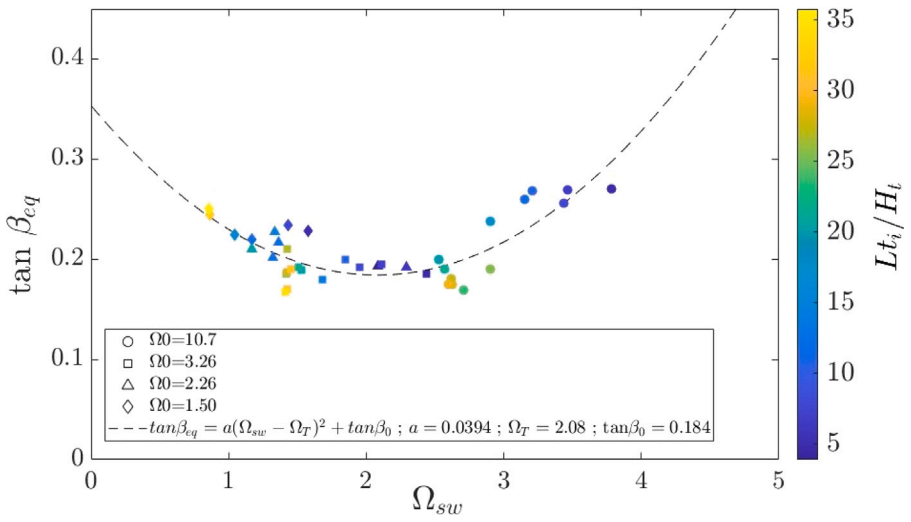

Fig. 8. Beach slope equilibrium value (β_{eq}) plotted against their associated Swash Dean number (Ω_{sw}) calculated at the bottom of the beach-face. Each symbol corresponds to one experiment and the colourmap corresponds to the initial beach slope position scaled by the water level on the terrace (Lt_i/H_i).

that included both sea and beach morphological surveys at both sites (Almar et al., 2017a, 2019a,b; Martins et al., 2017). The method for calculating the beachface slope evolution at NT and GP is described in Mingo et al. (2021), where the authors delineated the beachface slope as the linear segment between the berm crest point and the upper limit of the low tide terrace (see Fig. 9). This involved extracting a daily beachface slope for the entire survey period (2013 to 2016). Our physical device recreates this definition of the beachface slope in LTT environments (see Fig. 1).

As discussed in the Introduction 1 and in Section 2.4, both beaches (NT & GP) exhibit distinctly different wave climates, leading to contrasting hydro-morphodynamic behaviours within the inner-surf zone. However, they share a common characteristic of having a uniform low tide terrace and similar Dean number. Therefore, this dataset is well-suited to test our model and determine if it can accurately reproduce the beachface slope evolution on both cases. In Fig. 9, the mean summer and winter cross-shore beach profiles for Nha Trang and the annual cross-shore beach profile for Grand Popo are depicted, illustrating the LTT and the beachface slope (β).

Based on the previous correlation between the beachface slope and the swash Dean number from the physical model (see Fig. 8), we propose a quadratic law of $\beta_{eq}(\Omega_{sw})$ as

$$\tan\beta_{eq} = \alpha(\Omega_{sw} - \Omega_T)^2 + \tan\beta_0 \quad \text{with} \quad \alpha = 0.0394; \\ \Omega_T = 2.08; \quad \tan\beta_0 = 0.184 \tag{4}$$

The fitting coefficients of this equation are α, Ω_T and $\tan\beta_0$. Ω_T corresponds to a Dean transition from a swash-dominated to a surf-dominated beach system and β_0 is the associated beach face angle. A combination with Eqs. (1) and (3) leads to a simple model that allows to predict the rapid beach slope equilibrium induced by local wave action. This model reads :

$$\tan\beta_{eq} = \alpha\left(\left(\gamma_\infty + \exp\left[\sigma(x - x_0)/H_t\right]\right)\frac{H_t}{T_0 W_s} - \Omega_T\right)^2 + \tan\beta_0. \tag{5}$$

To make the model suitable for use with field data, a few simplifications and approximations are required. First, the transition $(\Omega_T, \tan\beta_0)$ is likely to be system and scale dependent. However, a transition between swash-dominated and surf-dominated has been found in field situations around a similar value of Dean number, $\Omega_0 \approx 2.5$, as recalled in Section 1. Then $\Omega_T = 2.08$ can be expected to remain relevant for field application. On the other hand, $tan\beta_0$, which corresponds to the minimum value of the beach slope obtained at the transition, is likely to be different between laboratory and field observations. This value depends strongly on the hydraulic regime of each system (wave sediment transport capacity). Adjustment of this parameter is therefore necessary for field data. In addition, the exact break location and dissipation law must be simplified to be useful for field application. It is suggested to simply combine $x_{sl} - x_0 = Lt$ regardless of the detailed role of x_0 in relation to (5). If the terrace length $L_t(t)$ is not available from field data, the relation $Lt \sim 0.4\lambda_0(t)$ suggested by Mingo et al. (2021) can be used instead. This approach leads to the derivation of a simplified model that can be tested on field data to predict the rapid evolution of beach slope. This can be written as :

$$\tan\beta_{eq} = \alpha\left(\left(\gamma_\infty + \exp\left[\sigma L_t/H_t\right]\right)\frac{H_t}{T_0 W_s} - \Omega_T\right)^2 + tan\beta_0, \tag{6a}$$

$$\tan\beta_{eq} = \alpha\left(\left(\gamma_\infty + \exp\left[0.4\lambda_0\sigma/H_t\right]\right)\frac{H_t}{T_0 W_s} - \Omega_T\right)^2 + tan\beta_0, \tag{6b}$$

with $\alpha = 0.0394$, $\sigma = 0.1318$, $\gamma_\infty = 0.3422$ and $\Omega_T = 2.08$, all fixed from the best fit of the physical model. The inputs from field measurements are thus the offshore wavelength and period (λ_0, T_0) and the sediment fall velocity W_s. For the model (6a), L_t is also an input from field measurements. Finally, two parameters remain adjustable for the (6a) and (6b) models. The first is the slope at the transition $\tan\beta_0$ as explained above. The second is the water depth above the terrace H_t. The latter parameter could be measured in the field. However, it mostly implies the dissipation law over the terrace, which could be strongly case dependent. Since this is the couple (σ, H_t), we propose here to adjust H_t, which varies strongly in the field due to tidal evolution and seasonal variations. Its evaluation can then be discussed with respect to the expected range of values from the field.

In the following, the models (6a) and (6b) are tested using the field data from Nha Trang and Grand Popo discussed in Section 1 and Mingo et al. (2021). These data include monthly mean measurements of beach slope β, terrace length L_t, and wave parameters (H_0, T_0, λ_0) over a period of 3.5 years. It was observed that for NT and GP the minimum slope is about 1/10. We therefore suggest $tan\beta_0 = 0.10$ as a first guess for the slope value at the transition. γ and σ correspond to the coefficients obtained from dissipation law on a flat platform (1). It should also be noted that several levels of H_t were tested to identify the optimal value of H_t that best described the field observations, as explained earlier. For Nha Trang, this value is $H_t = 1.1m$, which corresponds to the tidal range. For Grand Popo, the optimal mean water level on the terrace is $H_t = 3m$, which is almost twice as high as the maximum water depth during high tide. This difference could be attributed to the attenuation law used in the model, which is probably

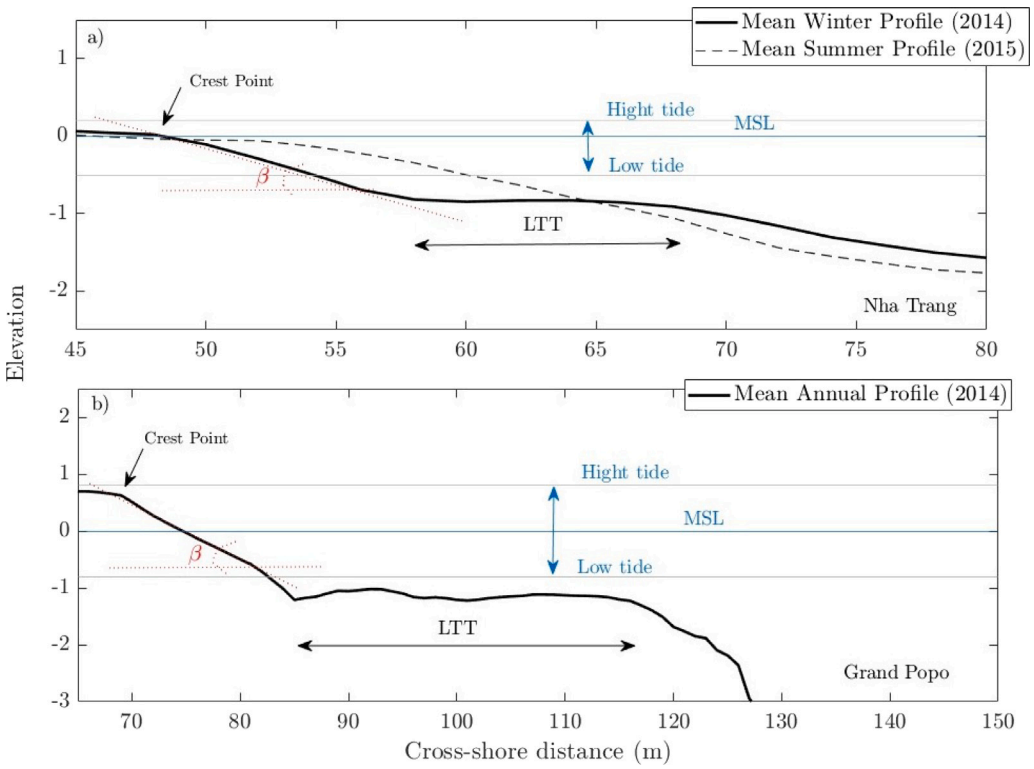

Fig. 9. Figure (a) depicts the winter and summer mean cross-shore beach profile at Nha Trang, while Figure (b) illustrates the annual cross-shore beach profile at Grand Popo. Both figures display the tidal levels, the LTT, and the beach face slope.

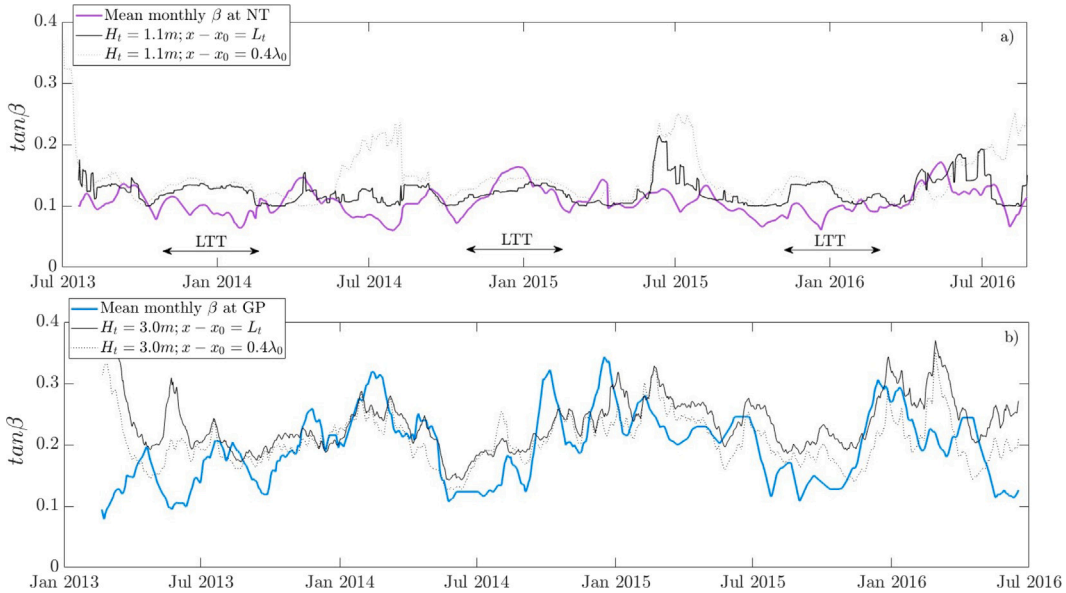

Fig. 10. (a) beach slope evolution at Nha Trang. The thick solid violet line corresponds to field observations, solid black line corresponds to the model results using the terrace length as in an input and dotted line corresponds to the model results using the relation 0.4λ instead of the terrace length as input. b) Same comparison than figure a but for Grand Popo, where field observation are represented with a thick solid blue line.

case-dependent, as the dissipation mechanism could be more complex than that obtained in the physical laboratory model.

The comparison of field data with the results obtained from the simplified models (6a)) and (6b) are shown in Fig. 10(a) for NT and in Fig. 10(b) for GP. In particular, field measurements are shown with blue and violet solid lines, black solid lines and black dashed lines corresponding to model (6a) and model (6b) respectively. The models show good agreement with both data sets (NT and GP). Although, the model performance may vary its ability to accurately predict the beach slope dynamics within each scenario, surf or swash control cases. In swash control cases, the model reproduces most of the beach slope changes to offshore wave forcing through significant and rapid fluctuations of the slope, as observed at GPP on the whole data set and at NT mostly during the summer seasons. In these cases, the role of the terrace remains small. However, the ability of the models to predict the evolution of the beach surface slope from a swash dominated to a surf dominated situation is quite good (see for example the decrease of

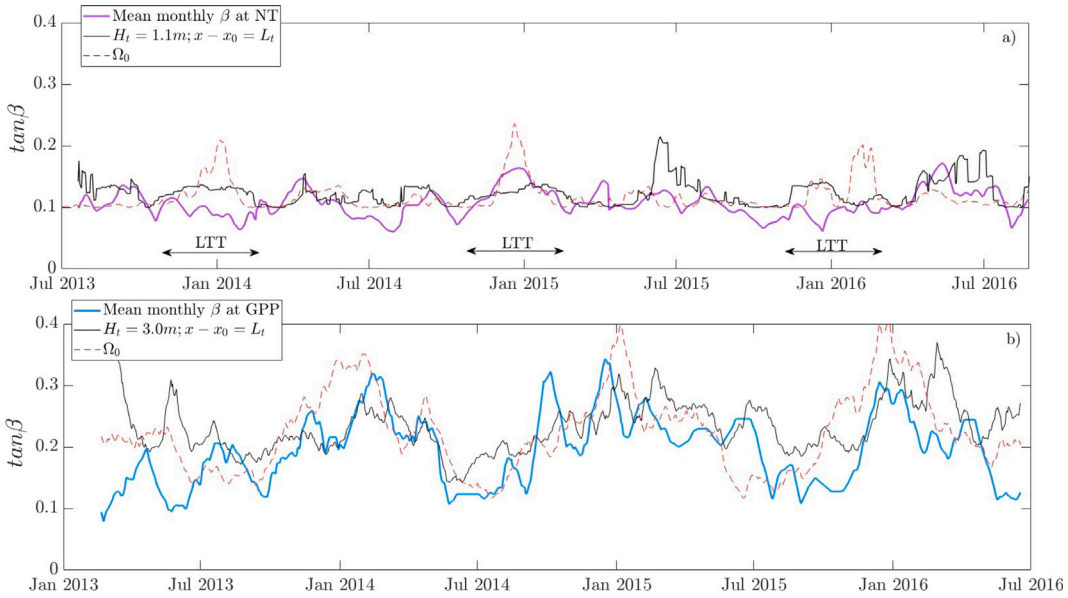

Fig. 11. (a) Beach slope evolution at Nha Trang. The thick solid violet line corresponds to field observations, solid black line corresponds to the model results using the Swash Dean number and the red dashed line corresponds to the model results using the off-shore Dean number instead of the Swash Dean number. (b) Same comparison than figure a but for Grand Popo, where field observation are represented with a thick solid blue line.

the slope from July 2015 to January 2016 at NT, for which the beach system evolves towards a terrace dominated regime).

Fig. 10 also highlights an important result regarding the influence of the distance from the breaking point to the beachface, as modelled by either the terrace length $L_t(t)$ (black solid line) or the relation $L_t \sim 0.4\lambda(t)$ (dotted line). Only a small difference between the models used for NT and GP is obtained, regardless of whether the distance is represented using $L_t(t)$ or $L_t \sim 0.4\lambda(t)$.

Note that for H_t additional studies are needed to fully evaluate the behaviour of the attenuation law under different water level conditions. However, as it was concluded that for swash control cases the beach slope responds directly to the offshore wave forcing, the wave height attenuation on the terrace could be neglected and the model could be tested directly with the offshore Dean number evolution Ω_0. This is shown in Fig. 11, where the dashed red line represents the evolution of the beach slope using the off-shore Dean number (Ω_0) instead of the swash Dean number (Ω_{sw}). This is advantageous because it simplifies the model and allows the evolution of the beach slope to be predicted using only offshore parameters such as wave height and period. However, it can be seen that some of the beach slope dynamics are lost when terrace dissipation is not taken into account. As an example of this, one can observe the difference in the prediction from July 2015 to January 2016 at NT (mentioned above). Obviously, the role of the terrace dissipation in the evolution of the beach slope at this stage of the morphological evolution, i.e. the increase of the terrace influence, is necessary to recover the observed decrease of the beach slope. A more accurate and dedicated evaluation of the models with field observations would deserve specific studies in the future.

4. Discussion

The laboratory-scale physical model described in this paper had three main objectives: (i) to highlight the rapid adjustment of the beach slope under wave action by quantifying the relationship between the offshore Dean number Ω_0 and the beach slope equilibrium β_{eq} on a short time scale, (ii) to understand and model the influence of inner-surf zone dissipation on this short time scale equilibrium state, using an idealized flat platform as a model of a terrace beach, an inner-surf zone influences the beach slope dynamics, and (iii) to compare obtained laboratory scale models with field data from two LTT environments. To this end, the inner-surf physical model was designed to highlight the specific influence of (Li_{sl}&β_i) to mimic either reflective, dissipative, or LTT environments. Depending on this initial geometry (Li_{sl}&β_i) and on the offshore wave forcing, it has been shown that the beach slope can either converge to an equilibrium value β_{eq}, referred to as the short time scale equilibrium state, or remain inactive. This rapid response must be seen as the beach slope equilibrium depending on both Li_{sl} and Ω_0, i.e. $\beta_{eq}(Li_{sl}, \Omega_0)$. Such an approach therefore allows to evaluate the slope of the beach face independent of the global erosion or accretion of the system.

4.1. Dean number interpretation

Our results from the inner-shore physical model show a relationship between β_{eq}, Li_{sl}, and Ω_0 that distinguishes two contrasting behaviours:

- For $\Omega_0 < 2.7$, β_{eq} is only weakly dependent on Li_{sl}, i.e. $\beta_{eq}(\Omega_0)$. This is referred to as an active swash system for which β_{eq} decreases for increasing Ω_0.
- For $\Omega_0 > 2.7$, the systems becomes surf-dominated, i.e. $\beta_{eq}(\Omega_0, Li_{sl})$, and the inner-surf length can not be disregarded.

The results allow to distinguish swash dynamics in a swash control or surf control environment, based either on offshore or swash zone wave conditions ($\Omega_0 < 2.7/\Omega_{sw} < 2.08$ and $\Omega_0 > 2.7/\Omega_{sw} > 2.08$ respectively). For the swash control beach ($\Omega_0 < 2.7$), the observed pattern of beach slope evolution suggests an inshore sediment flux, while for the surf control cases ($\Omega_0 > 2.7$) a constant beach face erosion was observed with constant sediment transport in offshore directions beyond the breaking point. This behaviour of the hydro-sedimentary systems is consistent with the Dean number interpretation, where small Ω_0 facilitates accretion while large Ω_0 leads to erosive morphodynamics.

The classification of swash and surf control beaches using the off-shore Dean number was proposed by Mingo et al. (2021) for two LTT beaches. Laboratory results support this classification, as the transition between these two states was found to be $\Omega_0 \approx 2.5$ in the field and $\Omega_0 \approx 2.7$ in the laboratory, suggesting a similar order of magnitude. However, it is worth mentioning an important limitation of this laboratory work and the field study conducted by Mingo et al. (2021) on the Dean number interpretation. In both laboratory and field, Ω_0 varies due to

the steepness of the wave type H_0/λ_0 and not due to the variation in sediment fall velocity. Therefore, further laboratory scale investigations are needed to clarify the role of Ω_0 and its interpretation as a control parameter of the swash dynamics.

4.2. Influence of a flat platform on beach slope dynamics

Low tide terrace environments are known to be tide-modified beaches that exhibit characteristics of both dissipative and reflective sites (Miles and Russell, 2004; Almar et al., 2016). At low tide, the terrace can be exposed to the surface and therefore there is no wave action on the upper beach face. As the water level on the terrace rises, lower levels favour wave breaking on the terrace, creating very dissipative conditions of the surf zone. On the contrary, it is suggested that during high tide, waves can pass unbroken over the terrace and act directly on the beach face, creating very reflective conditions (Lemos et al., 2018; Miles and Russell, 2004). Consequently, the water depth on the terrace, and consequently the wave dissipation along the inner surf, is a key parameter in LTT environments.

The innovative aspect of the inner-beach physical model used in this study is that it allows the simplification of these very complex hydro-sedimentary systems to a few key parameters. In particular, it allows to isolate and distinguish processes that are mostly coupled, such as β and Li_{sl}, and both with the offshore forcing. Here, the initial conditions (β_i, Li_{sl}) are varied independently of the off-shore forcing, leading to several states of the beach, from reflective to dissipative, with or without a significant influence of wave dissipation in the inner surf.

In order to quantify the influence of the terrace on the slope dynamics of the beach face, wave dissipation was modelled using the laboratory model. A dissipation law was found to be an exponential decay depending on the distance to the breaking point and the water depth above the terrace (see model (1)). Interestingly, it has been shown that the maximum bore amplitude along the terrace is only controlled by the water depth. This dissipation law has been incorporated into the definition of the Dean number to extract a local swash Dean number Ω (see Eq. (3)). This new definition allowed to rationalize the obtained beach slope equilibrium β_{eq}, which was thus shown to be a unique function of Ω_{sw} in the range of experimental parameters considered here. In particular, it shows a quadratic relationship between β_{eq} and Ω_{sw}, where $\Omega_{sw} = 2.08$ corresponds to a minimum slope. This critical value of $\Omega_{sw} = 2.08$ distinguishes the two different mechanisms of beach slope response, i.e., swash-controlled and surf-controlled.

- For $\Omega_{sw} < 2.08$, i.e. in the swash control case, $\beta_{eq}(\Omega_0 \approx \Omega_{sw})$ decreases with increasing Ω_0, i.e. Ω_{sw}.
- For $\Omega_{sw} > 2.08$, i.e. in the surf control situation, $\beta_{eq}(\Omega_0, Li_{sl} \rightarrow \Omega_{sw})$ increases with increasing Ω_{sw}.

4.3. Comparison of field observations of two LTT environments with physical model results

Finally, the results obtained from the physical model were compared with those obtained from field experiments carried out at two LTT beaches, Nha Trang and Grand Popo (Almeida et al., 2020; Thuan et al., 2019).

Grand Popo was classified as a swash control beach, with a good correlation between the monthly mean offshore Dean number Ω_0 and the monthly mean upper beach slope β. The Dean number at Grand Popo varied between 1.5 and 2.5 and the slope between $tan\beta = 0.1-0.3$, there was an inverse correlation between these two parameters (see figure 6 in paper Mingo et al., 2021). These field results agree well with the laboratory results for swash control cases, which have similar orders of magnitude as well as an inverse correlation between Ω_0 and β_{eq}. The physical laboratory experiments and GP show comparable morphodynamics, characterized by local morphological changes with no cross-shore sediment exchange beyond the inner-shore zone. This finding emphasizes the importance of individual wave action in regulating the dynamics of the upper beach slope over short time scales for swash control scenarios.

On the other hand, Nha Trang has been classified as a surf control beach by Mingo et al. (2021). Nha Trang shows a strong seasonal fluctuation where the beach continuously adapts to summer and winter wave conditions, distinguishing two clear phases: a LTT environment in winter and a more reflective state in summer. A robust correlation was found between the dynamics of the terrace length Lt (which appears and disappears according to the seasonal fluctuation) and the mean monthly Offshore Dean number Ω_0. However, the mean monthly dynamics of the beach surface slope β did not follow the monthly fluctuations of the offshore Dean number Ω_0. This suggests that the flat terrace acted as a filter to dissipate gravity waves, so that the beach slope did not respond directly to offshore wave action. The beach slope at Nha Trang varied around $tan\beta = 0.1$. In the laboratory, the lowest value of active beach slope generated by single waves on a short time scale was $tan\beta = 0.15$. This minimum value was reached when $\Omega_0 = 8.58$ (surf control) and a significant initial terrace length $Li_{sl}/H_t = 28$.

However, despite the quantitative differences between the results of the physical model and the field experiments at NT, two similar behaviours are observed. One is that the terrace acts as a low-pass filter. This has important consequences for the shortest waves (e.g. during storms) that might dissipate over the terrace, resulting in limited action on the beach face. The other similarity has to do with sediment transport, it is observed from the physical model that for surf control cases (high Dean numbers) the sediment was transported beyond the breaking zone in offshore directions, highlighting a strong cross-shore sediment exchange. While at NT, the morphological changes were observed mainly due to cross-shore sediment exchange transport beyond the inner-shore zones (Almeida et al., 2020).

The local Dean number, defined as the swash Dean number Ω_{sw}, is shown to be a relevant dimensionless parameter to refine the quantitative situation of the equilibrium beach slope β_{eq}. A parabolic relation between β_{eq} and Ω_{sw} (see Eq. (1)) allows to describe swash and surf control cases with a unique law (see Eq. (4)). From this laboratory relationship between β_{eq} and Ω_{sw}, a model is proposed to predict the evolution of the beach slope as a function of simple parameters, such as offshore wave period and wavelength (T_0 and λ_0), water depth on the terrace (H_t), and sediment fall velocity W_s (see Eqs. (6a) and (6b)). This beach slope model was tested using data from Nha Trang (NT) and Grand Popo (GP) beaches. The 3.5 year evolution of the monthly beach slope was reconstructed for both beaches using the model, and the results were compared with beach slope values obtained from field experiments (see Figs. 10 and 11). Although the comparison shows good agreement between the modelled and observed beach slope, indicating that the model is able to capture the dynamics of beach slope evolution at both NT and GP and to distinguish between surf and swash control situations, further testing is necessary to validate the model in other LTT micro-tidal environments.

5. Conclusion

This study presents a physical model for understanding the dynamics of beach slope evolution in reflective and LTT environments using a simplified approach of inner-shore hydro-sedimentary systems. The physical model is designed to capture an equilibrium beach slope β_{eq} on a short recovery time scale (individual wave action) for different monochromatic wave forcings. This is done by imposing a variety of initial beach morphology conditions, characterized by the inner surf zone length or terrace length Lt_i and the initial upper beach slope β_i. The results of this physical model allowed to classify the equilibrium beach slope as a function of the Dean number, based on either the offshore wave forcing (Ω_{sw}) or the local swash resulting flow characteristics (Ω_0). The results show that two situations can be distinguished:

a surf control or a swash control morphodynamics for $\Omega_0 > 2.7$ and $\Omega_0 < 2.7$, respectively. This definition is shown to be in agreement with field experiments carried out at two LTT beaches (Mingo et al., 2021).

The distinction between the off-shore and swash dean Ω_0 and Ω_{sw} was possible thanks to a hydrodynamic study carried out to examine the transformation of the waves on the flat platform, i.e. the modelled terrace, in order to quantify the wave energy dissipation. The main objective was to study the influence of the flat platform on the morphodynamics of the beach slope. In particular, it was observed that the wave breaking process when approaching the platform is depth controlled, i.e. the water level in the inner surf controls the maximum wave height and the dissipation after the breaking point. This process can be modelled by an exponential attenuation of the wave height away from the breaking point (see Eq. (1)). Such an evaluation allowed to propose a simple definition of the local swash Dean number, Ω_{sw}. It was shown to be a more relevant dimensionless number to characterize the morphodynamics in the surf control situation, i.e. $\Omega_0 > 2.7$, than the offshore Dean Ω_0. Thus, a simplified model is introduced to predict the rapid evolution of the beach slope as a function of the swash Dean number Ω_{sw}. The proposed model effectively describes the overall evolution of the beach slope on a short time scale, and highlights the distinction between swash and surf control scenarios. Further investigation is needed to improve our understanding of this phenomenon, including exploring the interpretation of the Dean number and investigating transient states that could lead to more refined out-of-equilibrium modelling.

Finally, the beach slope model together with the wave dissipation law into the inner-surf have proven relevance in describing swash and surf control for two LTT field situations, Gran-Popo and Nha Trang, given some parameter adjustments from physical models as explained along the paper. However, it remains unclear whether the law can be applied to other LTT environments. In particular, since water level is a critical parameter in the system, it is essential to investigate how the attenuation coefficients from the dissipation law change with varying water levels. Further studies are needed to clarify this aspect and to improve our understanding of wave dissipation on a flat platform. Nevertheless, this work is a starting point for explaining the variability of beach slopes observed in the field and has the potential to help improve our understanding of coastal morphodynamics.

The following abbreviations are used in this manuscript:

LTT	Low tide terrace
NT	Nha Trang
GP	Grand Popo
SRB	Surf regulated beach
SwRB	Swash regulated beach
Wr	Wave regime
s	Wave steepness
Ro	Rouse number
Ω_0	Dean number, calculated with off-shore wave parameters
Ω_{surf}	Surf Dean number, calculated with surf wave parameters
Ω_{sw}	Swash Dean number, calculated with local swash wave parameters
Ω_T	Transition Dean from swash-dominated to surf-dominated
H_0	Offshore wave height
T_o	Offshore wave period
λ_0	Offshore water wavelength
W_s	Sediment fall velocity
Lt_{sl}	Distance from the breaking point to the shoreline
L_t	Distance from the breaking point to the bottom of the beach face
x	Position on the channel aligned with wave propagation
X_0	shoreline retreat
β	beach slope
β_{eq}	Equilibrium beach slope
H_b	Maximal wave amplitude after the breaking processes
H_t	water depth on the terrace
D_{50}	mean sediment size
γ_{br}	Breaker index
γ_0	Breaker index at the beginning of the flat platform
γ_∞	Breaker index far away from the breaking point
σ	Fit coefficient (Spatial damping rate of the bore height due to friction)
α	fit coefficient

Funding

This research was funded by the French National Centre for Scientific Research (CNRS) through the 80 PRIME project (multi-team interdisciplinary research project).

CRediT authorship contribution statement

Ivana M. Mingo: Conceptualization, Data curation, Formal analysis, Investigation, Methodology, Writing – original draft. **Laurent Lacaze:** Investigation, Supervision, Validation, Writing – review & editing. **Rafael Almar:** Supervision, Writing – review & editing.

Declaration of competing interest

The authors declare that they have no known competing financial interests or personal relationships that could have appeared to influence the work reported in this paper.

Data availability

Data will be made available on request.

Acknowledgements

The authors would like to acknowledge Jean-Dominique Barron who played a crucial role in setting up the experimental device. His expertise and dedication were invaluable in ensuring the success of this work.

References

Abessolo Ondoa, G., Almar, R., Kestenare, E., Bahini, A., Houngue, G., Jouanno, J., Du Penhoat, Y., Castelle, B., Melet, A., Meyssignac, B., et al., 2016. Potential of video cameras in assessing event and seasonal coastline behaviour: Grand Popo, Benin (Gulf of Guinea). J. Coast. Res. (75 (10075)), 442–446.

Almar, R., Almeida, P., Blenkinsopp, C., Catalan, P., 2016. Surf-swash interactions on a low-tide terraced beach. J. Coast. Res. (75 (10075)), 348–352.

Almar, R., Blenkinsopp, C., Almeida, L.P., Bergsma, E.W., Catalan, P.A., Cienfuegos, R., Viet, N.T., 2019a. Intertidal beach profile estimation from reflected wave measurements. Coast. Eng. 151, 58–63.

Almar, R., Blenkinsopp, C., Almeida, L.P., Catalán, P.A., Bergsma, E., Cienfuegos, R., Viet, N.T., 2019b. A new remote predictor of wave reflection based on runup asymmetry. Estuar. Coast. Shelf Sci. 217, 1–8.

Almar, R., Blenkinsopp, C., Almeida, L.P., Cienfuegos, R., Catalan, P.A., 2017a. Wave runup video motion detection using the Radon Transform. Coast. Eng. 130, 46–51.

Almar, R., Hounkonnou, N., Anthony, E.J., Castelle, B., Senechal, N., Laibi, R., Mensah-Senoo, T., Degbe, G., Quenum, M., Dorel, M., et al., 2014. The Grand Popo beach 2013 experiment, Benin, West Africa: From short timescale processes to their integrated impact over long-term coastal evolution. J. Coast. Res. 70 (10070), 651–656.

Almar, R., Marchesiello, P., Almeida, L.P., Thuan, D.H., Tanaka, H., Viet, N.T., 2017b. Shoreline response to a sequence of typhoon and monsoon events. Water 9 (6), 364.

Almeida, L.P., Almar, R., Blenkinsopp, C., Senechal, N., Bergsma, E., Floc'h, F., Caulet, C., Biausque, M., Marchesiello, P., Grandjean, P., et al., 2020. Lidar observations of the swash zone of a low-tide terraced tropical beach under variable wave conditions: The Nha Trang (Vietnam) COASTVAR experiment. J. Mar. Sci. Eng. 8 (5), 302.

Anon, 2021. Wave Breaking. Delft University of Technology (Online accessed 09 February 2023).

Bagnold, R., 1940. Beach formation by waves: Some model experiments in a wave tank.(Includes photographs). J. Inst. Civ. Eng. 15 (1), 27–52.

Bakhtyar, R., Barry, D.A., Li, L., Jeng, D.S., Yeganeh-Bakhtiary, A., 2009. Modeling sediment transport in the swash zone: A review. Ocean Eng. 36 (9–10), 767–783.

Bascom, W.N., 1951. The relationship between sand size and beach-face slope. EOS Trans. Am. Geophys. Union 32 (6), 866–874.

Bernabeu, A., Medina, R., Vidal, C., 2003. A morphological model of the beach profile integrating wave and tidal influences. Mar. Geol. 197 (1–4), 95–116.

Briganti, R., Torres-Freyermuth, A., Baldock, T.E., Brocchini, M., Dodd, N., Hsu, T.J., Jiang, Z., Kim, Y., Pintado-Patiño, J.C., Postacchini, M., 2016. Advances in numerical modelling of swash zone dynamics. Coast. Eng. 115, 26–41.

Bruun, P., 1954. Coast Erosion and the Development of Beach Profiles, vol. 44, US Beach Erosion Board.

Bruun, P., 1962. Sea-level rise as a cause of shore erosion. J. Waterw. Harb. Div. 88 (1), 117–130.

Bujan, N., Cox, R., Masselink, G., 2019. From fine sand to boulders: Examining the relationship between beach-face slope and sediment size. Mar. Geol. 417, 106012.

Butt, T., Russell, P., 1999. Suspended sediment transport mechanisms in high-energy swash. Mar. Geol. 161 (2–4), 361–375.

Castelle, B., Marieu, V., Bujan, S., Ferreira, S., Parisot, J.-P., Capo, S., Sénéchal, N., Chouzenoux, T., 2014. Equilibrium shoreline modelling of a high-energy meso-macrotidal multiple-barred beach. Mar. Geol. 347, 85–94.

Chardón-Maldonado, P., Pintado-Patiño, J.C., Puleo, J.A., 2016. Advances in swash-zone research: Small-scale hydrodynamic and sediment transport processes. Coast. Eng. 115, 8–25.

Dally, W.R., Dean, R.G., 1984. Suspended sediment transport and beach profile evolution. J. Waterw. Port Coast. Ocean Eng. 110 (1), 15–33.

Dean, R.G., 1977. Equilibrium Beach Profiles: US Atlantic and Gulf Coasts. Department of Civil Engineering and College of Marine Studies, University of ...

Dean, R.G., 1991. Equilibrium beach profiles: characteristics and applications. J. Coast. Res. 53–84.

Guza, R.T., Thornton, E.B., 1982. Swash oscillations on a natural beach. J. Geophys. Res.: Oceans 87 (C1), 483–491.

Hughes, M.G., Masselink, G., Brander, R.W., 1997. Flow velocity and sediment transport in the swash zone of a steep beach. Mar. Geol. 138 (1–2), 91–103.

Kikkert, G.A., Pokrajac, D., O'Donoghue, T., Steenhauer, K., 2013. Experimental study of bore-driven swash hydrodynamics on permeable rough slopes. Coast. Eng. 79, 42–56.

Larson, M., Kubota, S., Erikson, L., 2004. Swash-zone sediment transport and foreshore evolution: field experiments and mathematical modeling. Mar. Geol. 212 (1–4), 61–79.

Lefebvre, J.P., Almar, R., Viet, N.T., Thuan, D.H., Binh, L.T., Ibaceta, R., Duc, N.V., 2014. Contribution of swash processes generated by low energy wind waves in the recovery of a beach impacted by extreme events: Nha Trang, Vietnam. J. Coast. Res. (70), 663–668.

Lemos, C., Floc'h, F., Yates, M., Le Dantec, N., Marieu, V., Hamon, K., Cuq, V., Suanez, S., Delacourt, C., 2018. Equilibrium modeling of the beach profile on a macrotidal embayed low tide terrace beach. Ocean Dyn. 68, 1207–1220.

Martins, K., Blenkinsopp, C.E., Almar, R., Zang, J., 2017. The influence of swash-based reflection on surf zone hydrodynamics: A wave-by-wave approach. Coast. Eng. 122, 27–43.

Masselink, G., Castelle, B., Scott, T., Dodet, G., Suanez, S., Jackson, D., Floc'h, F., 2016. Extreme wave activity during 2013/2014 winter and morphological impacts along the Atlantic coast of Europe. Geophys. Res. Lett. 43 (5), 2135–2143.

Masselink, G., Evans, D., Hughes, M.G., Russell, P., 2005. Suspended sediment transport in the swash zone of a dissipative beach. Mar. Geol. 216 (3), 169–189.

Masselink, G., Li, L., 2001. The role of swash infiltration in determining the beachface gradient: a numerical study. Mar. Geol. 176 (1–4), 139–156.

Masselink, G., Puleo, J.A., 2006. Swash-zone morphodynamics. Cont. Shelf Res. 26 (5), 661–680.

McCowan, J., 1891. VII. On the solitary wave. Lond. Edinb. Dublin Philos. Mag. J. Sci. 32 (194), 45–58.

Miche, M., 1944. Mouvements ondulatoires de la mer en profondeur constante ou décroissante. Ann. Ponts Chaussées (1) 26-78, (2) 270-292, (3) 369-406.

Miles, J., Russell, P., 2004. Dynamics of a reflective beach with a low tide terrace. Cont. Shelf Res. 24 (11), 1219–1247.

Mingo, I.M., Almar, R., Lacaze, L., 2021. Surf and swash dynamics on low tide terrace beaches. Coasts 1 (1), 73–89. http://dx.doi.org/10.3390/coasts1010005.

Pritchard, D., Hogg, A.J., 2005. On the transport of suspended sediment by a swash event on a plane beach. Coast. Eng. 52 (1), 1–23.

Puleo, J.A., 2009. Tidal variability of swash-zone sediment suspension and transport. J. Coast. Res. 25 (4), 937–948.

Puleo, J., Holland, K., Plant, N., Slinn, D., Hanes, D., 2003. Fluid acceleration effects on suspended sediment transport in the swash zone. J. Geophys. Res.: Oceans 108 (C11).

Reis, A.H., Gama, C., 2010. Sand size versus beachface slope—an explanation based on the constructal law. Geomorphology 114 (3), 276–283.

Short, A.D., 1996. The role of wave height, period, slope, tide range and embay-mentisation in beach classifications: a review. Revista Chil. Hist. Nat. 69 (4), 589–604.

Soares, A.G., 2003. Sandy Beach Morphodynamics and Macrobenthic Communities in Temperate, Subtropical and Tropical Regions: A Macroecological Approach (Ph.D. thesis). University of Port Elizabeth.

Steenhauer, K., Pokrajac, D., O'Donoghue, T., 2012. Numerical model of swash motion and air entrapment within coarse-grained beaches. Coast. Eng. 64, 113–126.

Sunamura, T., 1984. Quantitative predictions of beach-face slopes. Geol. Soc. Am. Bull. 95 (2), 242–245.

Thuan, D.H., Almar, R., Marchesiello, P., Viet, N.T., 2019. Video sensing of nearshore bathymetry evolution with error estimate. J. Mar. Sci. Eng. 7 (7), 233.

Turner, I.L., 1995. Simulating the influence of groundwater seepage on sediment transported by the sweep of the swash zone across macro-tidal beaches. Mar. Geol. 125 (1–2), 153–174.

Turner, I.L., Russell, P.E., Butt, T., 2008. Measurement of wave-by-wave bed-levels in the swash zone. Coast. Eng. 55 (12), 1237–1242.

Van Rijn, L.C., 1993. Principles of sediment transport in rivers, estuaries and coastal seas.

Wright, L., May, S., Short, A., Green, M., 1984. Beach and surf zone equilibria and response times. In: Coastal Engineering 1984. pp. 2150–2164.

Yates, M.L., Guza, R., O'reilly, W., 2009. Equilibrium shoreline response: Observations and modeling. J. Geophys. Res.: Oceans 114 (C9).